


## Polarized Light from the Transportation of a Matter-Antimatter Beam in a Plasma

Ujjwal Sinha, Christoph H. Keitel, and Naveen Kumar\*

*Max-Planck-Institut für Kernphysik, Saupfercheckweg 1, D-69117 Heidelberg, Germany*

 (Received 17 December 2018; revised manuscript received 26 March 2019; published 21 May 2019)

A relativistic electron-positron beam propagating through a magnetized electron-ion plasma is shown to generate both circularly and linearly polarized synchrotron radiations, which is intrinsically linked with asymmetric energy dissipation of the pair beam during the filamentation instability dynamics in the background plasma. The ratio of both polarizations  $|\langle P_{\text{circ}} \rangle / \langle P_{\text{lin}} \rangle| \sim 0.15$ , occurring for a wide range of beam-plasma parameters, can help in understanding the recent observation of circularly polarized radiation from gamma-ray bursts.

DOI: [10.1103/PhysRevLett.122.204801](https://doi.org/10.1103/PhysRevLett.122.204801)

Radiation from extreme astrophysical scenarios such as, e.g., gamma-ray bursts (GRBs) occurring in supernova explosions, pulsar wind nebulae, and active galactic nuclei is of immense interest as it holds vital clues about the origin of these astrophysical scenarios and acceleration of cosmic rays [1–4]. GRBs are one of the unsolved problems in astrophysics, and they are capable of releasing enormous amount of energy ( $E_k \sim 10^{51}$  erg) in a small volume of radius  $\sim 10^3$  km [5]. Thus, one can expect a copious amount of pair plasma ( $e^-$ ,  $e^+$ ) being generated, which is termed as a fireball that propagates in the plasma made of baryonic matter [6]. This can give rise to the onset of plasma instabilities, notably the Weibel or current filamentation instabilities (WI/CFIs) [7] that can generate a strong magnetic field, converting the kinetic energy of the streaming particle into electromagnetic fields [8,9]. Both the pair plasma and the relativistic ejecta of supernova explosion are capable of launching internal and external (with the interstellar medium) collisionless shocks, respectively. These shocks can accelerate the baryonic matter to high energy and can be responsible for the ultrahigh energy cosmic rays. The presence of a strong magnetic field can cause ultrarelativistic particles to emit synchrotron radiation. Indeed, the radiation signatures from GRBs indicate the presence of strong equipartition magnetic field [3,10,11]. Moreover, the radiation is deemed to be linearly polarized [12–14]. However, recent observation of the circular polarization (CP) radiation [2] in the afterglow of GRBs calls for studying the polarization properties of the radiation from GRBs and the role of plasma composition and dynamics on the synchrotron radiation emission [15–17].

Parallel to the observations of astrophysical processes from ground-based and airborne telescopes, there has also been a growing interest in utilizing powerful and highly energetic laser systems [18–22] to study collisionless shocks, magnetic reconnection, and plasma instability dynamics in a controlled laboratory experiment [20,23–28]. It is a rapidly

evolving area of research known as laboratory astrophysics, which invokes the similarity principle to felicitate comparison between the laboratory experiments and the astrophysical scenarios [29]. Recently, a breakthrough experiment was conducted in which a dense pair-plasma beam of density  $n_b \sim 10^{16}$  cm $^{-3}$  with an average Lorentz factor  $\gamma_{\text{av}} \approx 15$  was produced in a laboratory [24]. The generation of neutral high-density pair plasma is very encouraging as it can attempt to give insight into the transport of matter-antimatter beam in a plasma, mimicking the conditions of the fireball beam propagation in GRBs.

Motivated by these developments, in this Letter, we study the polarized radiation from propagation of a pair plasma in a magnetized electron-ion plasma by three-dimensional (3D) particle-in-cell (PIC) simulations. Here, the case of magnetized scenario is important as the polarization of GRBs indicates the presence of an ordered magnetic field [1,2]. The motives for our study are twofold: First, it is analogous to the finite fireball beam propagation in a magnetized background plasma of baryonic matter. Second, it complements the ongoing experimental efforts in laboratory astrophysics, where the proton radiography technique is heavily used to map the field strength and particle densities [23,27]. Polarized radiation from plasma particle can also serve an important role in deciphering the dynamics of plasma instabilities, complementing the proton radiography technique.

Full 3D PIC simulations on the propagation of a cold relativistic pair beam ( $e_b^-$ ,  $e_b^+$ ) in a preformed magnetized uniform electron-proton plasma are carried out with PIC code SMILEI [30]. A moving (in  $x$  direction) simulation window of size  $[16 \times 32 \times 32](c/\omega_p)^3$  with resolutions of  $[256 \times 256 \times 256]$  cells with absorbing boundary conditions for particles and fields in the transverse direction was used. Here  $\omega_p = (4\pi n_0 e^2 / m_e)^{1/2}$  is the electron plasma frequency of the ambient electron-proton plasma,  $n_0$  the electron density,  $e$  and  $m_e$  are the electronic charge and mass, respectively, and  $c$  is the velocity of the light in

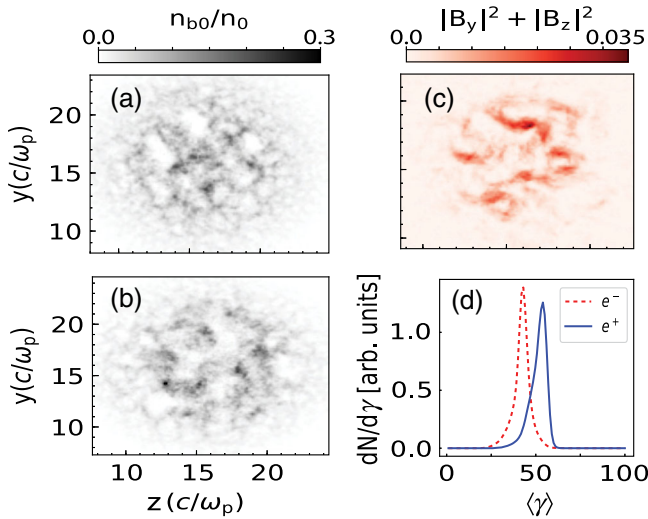


FIG. 1. (a),(b)  $e_b^-$  and  $e_b^+$  densities in the  $yz$  plane, respectively, at  $x = 8c/\omega_p$ . (c) Spatial distribution of transverse magnetic field energy in the  $yz$  plane at  $x = 8c/\omega_p$ . (d) beam  $e_b^-$  (dotted red) and the beam  $e_b^+$  (solid blue) energy distribution showing the deceleration of  $e_b^-$  and acceleration of  $e_b^+$ .

vacuum. The pair beam has a Gaussian profile with full width at half-maximum  $[2 \times 8.5 \times 8.5](c/\omega_p)^3$ . A timestep of  $\Delta t = 0.0295\omega_p^{-1}$  and  $[2 \times 2 \times 2]$  particles per cell per species were used [31]. The ambient plasma has a temperature  $\sim 5$  keV, and was magnetized with a uniform magnetic field  $\mathbf{B}_0 = B_0 \hat{\mathbf{e}}_x$ , of varying strengths  $B_0 \sim (3-30)$  T, which is available for current laboratory astrophysics experiments. The external magnetic field can correspond to either the magnetic field of central engine of GRBs, interstellar magnetic field compressed at the shock front, or field generated due to other dynamical processes [6,14,17,32].

When a pair beam ( $e_b^-, e_b^+$ ) propagates in a plasma, the beam electrons ( $e_b^-$ ) repel and the beam positrons ( $e_b^+$ ) attract the background plasma electrons, respectively, violating the quasineutrality of the plasma. This causes the generation of an inductive electric field that, in turn, generates a return plasma current to neutralize the effect of external beam. Since the pair beam has transverse size larger than the plasma skin-depth  $d_s = c/\omega_p$ , the return plasma current can penetrate and flow inside the pair beam. This configuration of the opposite beam currents is unstable in a plasma, and it can split the pair beam into smaller filaments of size  $\sim d_s$  due to the WICFI mechanism, leading to the generation of a strong transverse magnetic field at the expense of the pair-beam energy. Since in the case of an ambient electron-proton plasma, only the background electrons participate in the current neutralization as  $m_p \gg m_e$ , the  $e_b^+$  and  $e_b^-$  filaments experience acceleration and deceleration, respectively, leading to the difference in their energy spectrum [33]. Figures 1(a) and 1(b) show density of the beam species with the density  $n_{b0} = 0.1n_0$  and the Lorentz factor  $\gamma = 50$  after

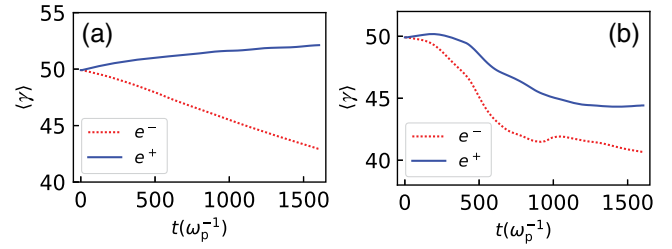


FIG. 2. Energy dissipation of each species at (a)  $n_{b0}/n_0 = 0.1$  and (b)  $n_{b0}/n_0 = 1$ . Other parameters are same as in Fig. 1.

propagating a distance of  $1500 c/\omega_p$  (50 cm for  $n_0 = 10^{16} \text{ cm}^{-3}$ ) in an initially magnetized ( $B_0 = 7.5$  T) electron-proton plasma. One can see the filamentation of the pair beam due to the WICFI in panels (a) and (b) and associated magnetic field energy in panel (c). Figure 1(d) shows the difference in average kinetic energies (normalized by  $m_e c^2$ ) between the beam  $e_b^+$  and  $e_b^-$  which is  $\langle \gamma \rangle_{e_b^+} - \langle \gamma \rangle_{e_b^-} \approx 10$ . This energy difference ( $\sim 5$  MeV) is predominantly caused by the beam energy loss in generating the magnetic field, but also due to the return current neutralization dynamics. Figure 2 shows that for density ratio  $n_{b0}/n_0 = 0.1$ , the  $e_b^-$  loses energy while  $e_b^+$  gains energy as explained before. However, at density ratio  $n_{b0}/n_0 = 1$ , both species lose energy to generate the magnetic field due to the WICFI, though the  $e_b^+$  population still has higher average energy than the  $e_b^-$  population. Indeed, the beam to magnetic field energy conversion ratios in both cases read 2% for  $n_{b0}/n_0 = 0.1$  and 4.7% for  $n_{b0}/n_0 = 1$ . This suggests that  $e_b^-$  population dominantly contributes to the magnetic field generation. This can be simply understood by observing the fact that both the  $e_b^+$  and return plasma currents are in the same direction, and hence they are not as unstable as the oppositely moving  $e_b^-$  and return plasma currents.

We have developed a new postprocessing code CASPER [34] that employs the method of Fourier transform of the radiated electric field and the Stokes parameters [4,35–37]. A two-dimensional virtual detector of size  $[30000 \times 30000](c/\omega_p)^2$  is kept in the  $yz$  plane at a distance  $x = 10^5(c/\omega_p)$ , having  $50 \times 50$  grid points. The frequency range  $\omega = (10^0-10^3)\omega_p$  (large enough for the spectrum) is analyzed with a resolution of  $\Delta\omega = 1$ . Trajectories of particles, randomly selected from the  $xy$  plane at  $z = 16c/\omega_p$ , are extracted from the PIC simulations [38]. On defining  $\mathbf{e}_1$  and  $\mathbf{e}_2$  as the unit vectors perpendicular to the direction of observation and  $\mathbf{E}$  as the resultant radiated electric field vector from all the charged particles, the Stokes parameters are given as  $s_0 = |\mathbf{e}_1 \cdot \mathbf{E}|^2 + |\mathbf{e}_2 \cdot \mathbf{E}|^2$ ;  $s_1 = |\mathbf{e}_1 \cdot \mathbf{E}|^2 - |\mathbf{e}_2 \cdot \mathbf{E}|^2$ ;  $s_2 = 2\text{Re}[(\mathbf{e}_1 \cdot \mathbf{E})^*(\mathbf{e}_2 \cdot \mathbf{E})]$ ;  $s_3 = 2\text{Im}[(\mathbf{e}_1 \cdot \mathbf{E})^*(\mathbf{e}_2 \cdot \mathbf{E})]$  [13,39]. The total linear and circular polarizations read as  $\langle P_{\text{lin}} \rangle = \langle \sqrt{s_1^2 + s_2^2}/s_0 \rangle$  and  $\langle P_{\text{circ}} \rangle = \langle s_3/s_0 \rangle$ , respectively, where  $\langle s_i/s_0 \rangle = \iint s_i dA d\omega / \iint s_0 dA d\omega$  with  $A$  as the area of the detector and  $i = (1, 2, 3)$  [40]. Figures 3(a) and 3(b) show

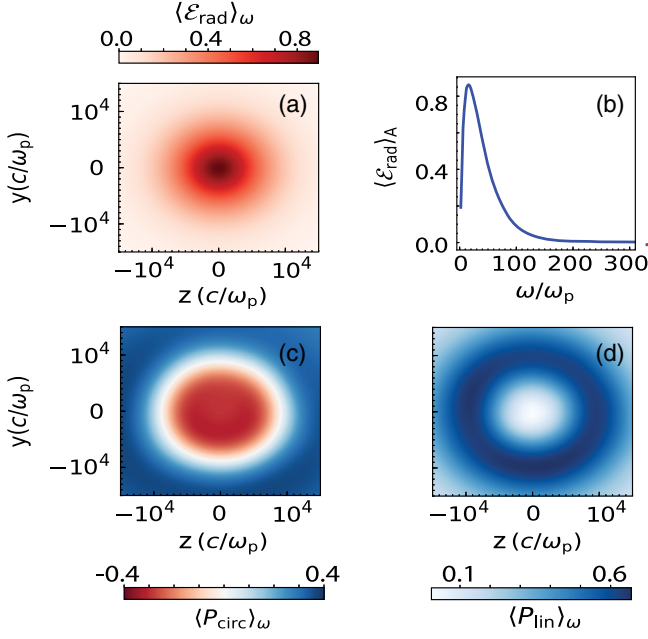


FIG. 3. Computation of radiation from CASPER using 8000 beam  $e_b^-$  and  $e_b^+$  particles during the time between  $t_i = 750\omega_p^{-1}$  to  $t_f = 1500\omega_p^{-1}$  for  $n_{b0}/n_0 = 0.1$  and  $\gamma = 50$ . (a),(b) Frequency and space averaged radiated energy, respectively, from the beam species. The frequency and space averages are denoted by the subscripts  $\omega$  and  $A$ , respectively. The  $\langle \mathcal{E}_{\text{rad}} \rangle$  is normalized to  $4\pi^2 c/e^2$ . Frequency averaged  $\langle P_{\text{circ}} \rangle$  in panel (c) and  $\langle P_{\text{lin}} \rangle$  in panel (d).

the radiated energy and frequency corresponding to Fig. 1. The spectrum confirms the emission to be a synchrotron process. Since the  $e_b^+$  and  $e_b^-$  populations have an energy difference and for a charged particle with Lorentz factor  $\gamma$ , the total energy radiated scales as  $\mathcal{E}_{\text{rad}} \propto \gamma^4$  [13], the CP radiation flux (caused by  $\mathbf{B}_0$ ) due to beam  $e_b^+$  exceeds the radiation flux from beam  $e_b^-$ . This can also be confirmed by comparing Figs. 3(c) and 3(d) where regions of high degree of circular polarization show small amount of linear polarization. The frequency averaged degree of circular and linear polarizations with peak values of  $\langle P_{\text{circ}} \rangle_{\omega} \approx 0.4$  (40%) and  $\langle P_{\text{lin}} \rangle_{\omega} \approx 0.6$  (60%) are shown in Figs. 3(c) and 3(d), respectively. The total fractional linear and circularly polarized radiation fluxes [integrated over the

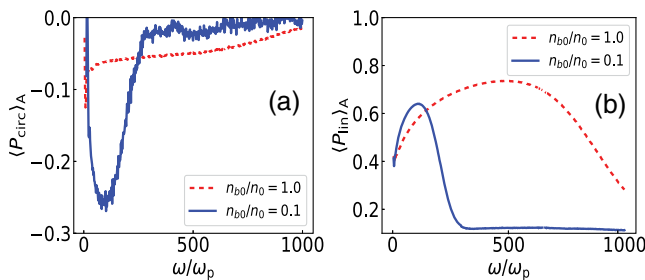


FIG. 4. Frequency spectra of the polarized radiation for two cases of beam to plasma density ratios.

whole area in Figs. 3(c) and 3(d) are  $\langle P_{\text{circ}} \rangle \approx 0.18$  (18%) and  $\langle P_{\text{lin}} \rangle \approx 0.49$  (49%), respectively. In all cases, polarized light is found to be  $\sim(67-69)\%$ , making the fraction of unpolarized light to be  $\sim(33-31)\%$ . Figure 4 shows the spectrum of the  $\langle P_{\text{circ}} \rangle$  and  $\langle P_{\text{lin}} \rangle$  peaks at  $\omega \approx 100\omega_p$  for  $n_{b0} = 0.1n_0$ , which corresponds to a wavelength of  $\sim 3 \mu\text{m}$  (far infrared) for  $n_0 = 10^{16} \text{ cm}^{-3}$  [41].

We use synchrotron radiation formalism [13] to calculate the degree of polarization analytically and compare it with PIC simulations. Numerically integrating the Stokes parameters  $s_3$  and  $s_0$  for the radiated field over the entire solid angle and the frequency range (see the Supplemental Material [38]) for the pair beam with distribution functions from PIC simulations,  $f(\gamma)_\alpha$ , where  $\alpha = (e_b^-, e_b^+)$ , the resultant degree of circular polarization  $\langle P_{\text{circ}} \rangle = (\langle P_{\text{cflux}} \rangle_{e_b^-} - \langle P_{\text{cflux}} \rangle_{e_b^+}) / (\langle \mathcal{E}_{\text{rad}} \rangle_{e_b^-} + \langle \mathcal{E}_{\text{rad}} \rangle_{e_b^+})$ , where  $\langle P_{\text{cflux}} \rangle_\alpha = \int P_{\text{cflux}} f(\gamma)_\alpha d\gamma / \int f(\gamma)_\alpha d\gamma$ , yields

$$\langle P_{\text{circ}} \rangle = 0.8415 \frac{\langle \gamma^4 \rangle_{e_b^-} - \langle \gamma^4 \rangle_{e_b^+}}{\langle \gamma^4 \rangle_{e_b^-} + \langle \gamma^4 \rangle_{e_b^+}}. \quad (1)$$

We performed and compared two sets of simulations with Eq. (1): First, with  $n_{b0}/n_0 = [0.1, 0.25, 0.5, 0.75, 1.0]$  for a fixed beam Lorentz factor  $\gamma = 50$ , and with  $\gamma = [10, 20, 30, 40, 50]$  at a fixed density ratio  $n_{b0}/n_0 = 1.0$ . The  $\langle \gamma^4 \rangle_\alpha$  of each beam species was calculated for the duration  $(750-1500)\omega_p^{-1}$  using the density distribution obtained from the simulation data. The  $\langle P_{\text{circ}} \rangle$  followed the scaling of Eq. (1) as shown in Figs. 5(a) and 5(b). The  $\langle P_{\text{circ}} \rangle$  decreases while the  $\langle P_{\text{lin}} \rangle$  (insets) increases with  $n_{b0}/n_0$ . Since asymmetric energy dissipation in  $e_b^+$  and  $e_b^-$  species is larger at low density (as seen in Fig. 2), the CP flux is also higher at lower densities. At higher density the energy difference between beam species is lower, yielding strong linear polarization as expected from synchrotron

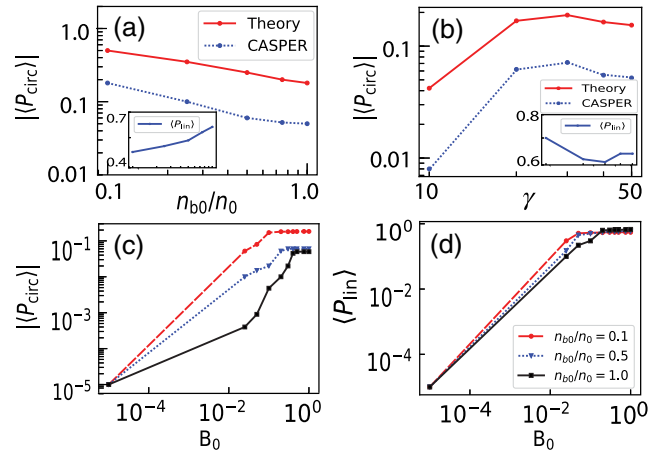


FIG. 5. Scalings of  $\langle P_{\text{circ}} \rangle$  from Eq. (1) and PIC simulations (with 2000 particles). Scaling of the  $|\langle P_{\text{circ}} \rangle|$  and  $\langle P_{\text{lin}} \rangle$  (inset) (a) at  $\gamma = 50$ , (b) at initial  $n_{b0}/n_0 = 1.0$ . For (a) and (b),  $B_0 = 1$  (normalized by  $m_e \omega_p c/e$ ). Panels (c) and (d) show the scalings of  $\langle P_{\text{circ}} \rangle$  and  $\langle P_{\text{lin}} \rangle$  with  $B_0$  at  $n_{b0} = [0.1, 0.5, 1.0]$  and initial  $\gamma = 50$ .



emission [12,14]. Contrastingly,  $\langle P_{\text{circ}} \rangle$  increases ( $\langle P_{\text{lin}} \rangle$  decreases) with  $\gamma$ , peaks around  $\gamma = 30$  and decreases afterward as shown in Fig. 5(b) for density ratio  $n_{b0}/n_0 = 1$ . The decrease can be associated with the effect of plasma hosing and modulation instabilities in plasma wakefield regime which may further reduce and saturate  $\langle P_{\text{circ}} \rangle$  for high beam densities. Figures 5(c) and 5(d) show the dependence on the external magnetic field  $B_0$  for different  $n_{b0}/n_0$ . Both components of polarizations increase with  $B_0$  and saturate when the WI/CFI generated magnetic field equals the external magnetic field. The WI/CFI fields add a degree of randomness to the motion of charged particles reducing  $\langle P_{\text{circ}} \rangle$  and  $\langle P_{\text{lin}} \rangle$ . For high  $B_0$ , the motion of the beam particles is dominated by  $B_0$  and  $\langle P_{\text{circ}} \rangle$  arises only due to the energy difference between the beam  $e_b^-$  and  $e_b^+$  as seen in Figs. 5(c) and 5(d). In case of an  $e_b^-$ ,  $e_b^+$  ambient plasma, both the species of the ambient plasma contribute equally to neutralize the current filaments of the beam species. As a result, there is no asymmetry in the kinetic energies between the beam species. Then  $\langle P_{\text{circ}} \rangle = 0$  for such a case and is independent of  $n_{b0}/n_0$ , because the  $\langle P_{\text{circ}} \rangle$  due to the beam  $e_b^-$  is canceled by that due to the beam  $e_b^+$ ; see also Ref. [16] where generation of circular polarization in a different physical configuration is attributed to the topological changes in pitch-angle distribution of electrons instead of the asymmetric energy dissipation discussed here.

To discuss the relevance of our results in the context of GRBs, we invoke the similarity principle [29]. Since we explore the degree of polarization which is a dimensionless quantity, thus one can use the scaling argument and compare the characteristic length and the time in laboratory and astrophysical scenarios [29]. In our case, these scales are the electron plasma skin depth,  $\sim c/\omega_p$ , and electronic plasma frequency,  $\omega_p$ , respectively. Thus, the laboratory scale length  $L_1$  and time  $t_1$  can be related with the corresponding astrophysical time ( $t_A$ ) and length ( $L_A$ ) as  $t_A = t_1 \sqrt{n_0/n_A}$  and  $L_A = L_1 \sqrt{n_0/n_A}$ , where  $n_A$  is the typical plasma density in the astrophysical scenario. On taking  $n_0 = 10^{16} \text{ cm}^{-3}$  [24] and  $n_A = 1 \text{ cm}^{-3}$  [42], we obtain for our parameters  $t_A = 1.1 \times 10^{-4} \text{ s}$  and  $L_A = 5.33 \times 10^5 \text{ cm}$ . These scales are smaller than the values often cited for GRBs [6,17], thus indicating that the WI/CFI mechanism has ample time and spatial extent to grow and affect the radiation generation. Similarly, the external magnetic field used in our PIC simulations (scales as  $B_A = B_1 \sqrt{n_A/n_0}$ ) falls in the range  $\sim (0.3-3) \text{ mG}$  for  $n_A = 1 \text{ cm}^{-3}$ , consistent with the field associated with GRBs [43]. For the beam propagation time (yielding the polarized light in the laboratory)  $t_1 = 2.66 \times 10^{-10} \text{ s}$  ( $1500\omega_p^{-1}$ ), the corresponding time  $t_A = 2.66 \times 10^{-2} \text{ s}$  is within the time range  $\sim (0.01-100) \text{ s}$  reported for GRBs [6]. Notably, we find that the ratio  $|P_{\text{circ}}/P_{\text{lin}}| \sim 0.15$  (for  $n_{b0}/n_0 = [0.25, 0.50]$  with  $\gamma = 50$

and for  $n_{b0}/n_0 = 1.0$  with  $\gamma = 30$  in infrared frequency range) is close to the value reported by Wiersema *et al.* [2]. Though other processes such as Faraday rotation can also cause the generation of circular polarization [17], spectra of radiation differs in each case. Moreover, Nava *et al.* [15] have recently argued that the ratio  $|P_{\text{circ}}/P_{\text{lin}}| \sim 0.15$  reported by Wiersema *et al.* [2] cannot be explained by the pitch-angle anisotropy and conclude that Lorentz factor has to be small,  $P_{\text{circ}} \sim 1/\gamma$ . However, our results show the observed value of  $|P_{\text{circ}}/P_{\text{lin}}| \sim 0.15$  for a wider beam to plasma density ratios and higher fireball beam Lorentz factors. This further signifies the hitherto unexplored role of the plasma instabilities (WI/CFI) on the circular polarization generation in GRBs. Moreover, the scaling introduced in Eq. (1) can also be exploited for use in subgrid-model of astrophysical simulations. One may also note that we have not included electron-positron annihilation, radiation reaction effects, and plasma collisions in the PIC simulations. The annihilation rate in a plasma, in the ultrarelativistic limit is  $\dot{n}_+ = (2\pi c n_+ n_- r_e^2 / \gamma) [\ln(2\gamma) - 1] \text{ s}^{-1}$ , where  $n_+$ ,  $n_-$  are the electron and positron densities respectively,  $r_e$  is the classical electron radius, and  $\gamma$  is the Lorentz factor of the pair beam [44]. For PIC simulation parameters,  $n_+ = n_- = 10^{15} \text{ cm}^{-3}$ , beam volume of  $5.7 \times 10^{-4} \text{ cm}^3$ , and  $\gamma = 50$ , the annihilation rate implies loss of only  $10^5$  particles out of total  $10^{11}$  beam particles (at the end of simulation) justifying the assumption of ignoring the pair annihilation in our PIC simulations. Also, the magnetic field due to the WI does not grow to large values to necessitate the inclusion of RR force in our PIC simulations [45].

In conclusion, we have shown that a pair beam ( $e_b^-$ ,  $e_b^+$ ) propagating through a magnetized electron-proton plasma suffers asymmetric energy dissipation due to the generation of the transverse magnetic field caused by the WI/CFI mechanism. The asymmetric energy dissipation does not allow the left and right circularly polarized radiation fluxes from the beam species to cancel, resulting in a finite circularly polarized radiation flux. The degrees of linear and circular polarizations depend on ratio  $n_{b0}/n_0$ ,  $\gamma$  of the fireball beam, and the external magnetization. These results can be readily tested in laboratory astrophysics experiments. In addition, the origin of circular polarization due to asymmetric energy dissipation between beam  $e_b^-$  and  $e_b^+$  species highlights the importance of the plasma instabilities in the recently observed circular polarization in optical frequency range in GRBs [2].

The authors would like to thank Dr. K. Hatsagortsyan for useful discussions. U.S. would like to thank the SMILEI development team for technical support.

\*Corresponding author.

naveen.kumar@mpi-hd.mpg.de

[1] C. Mundell *et al.*, *Nature (London)* **504**, 119 (2013).

- [2] K. Wiersema *et al.*, *Nature (London)* **509**, 201 (2014).
- [3] D. Band *et al.*, *Astrophys. J.* **413**, 281 (1993).
- [4] C. Hededal, [arXiv:astro-ph/0506559](https://arxiv.org/abs/astro-ph/0506559).
- [5] T. Piran, Toward understanding gamma-ray bursts, in *Unsolved Problems in Astrophysics*, edited by J. N. Bahcall and J. P. Ostriker (Princeton University Press, Princeton, New Jersey, 1997), pp. 343–369.
- [6] T. Piran, *Rev. Mod. Phys.* **76**, 1143 (2005).
- [7] E. S. Weibel, *Phys. Rev. Lett.* **2**, 83 (1959).
- [8] L. O. Silva, R. A. Fonseca, J. W. Tonge, J. M. Dawson, W. B. Mori, and M. V. Medvedev, *Astrophys. J. Lett.* **596**, L121 (2003).
- [9] P. Muggli, S. Martins, N. Shukla, J. Vieira, and L. Silva, [arXiv:1306.4380](https://arxiv.org/abs/1306.4380).
- [10] M. C. Begelman, R. D. Blandford, and M. J. Rees, *Rev. Mod. Phys.* **56**, 255 (1984).
- [11] R. D. Blandford and R. L. Znajek, *Mon. Not. R. Astron. Soc.* **179**, 433 (1977).
- [12] G. B. Rybicki and A. P. Lightman, *Radiative Processes in Astrophysics* (Wiley-VCH Verlag GmbH & Co. KGaA, Weinheim, 2004).
- [13] J. D. Jackson, *Classical Electrodynamics*, 3rd ed. (John Wiley & Sons, New York, 1999).
- [14] M. V. Medvedev and A. Loeb, *Astrophys. J.* **526**, 697 (1999).
- [15] L. Nava, E. Nakar, and T. Piran, *Mon. Not. R. Astron. Soc.* **455**, 1594 (2016).
- [16] U. Sinha, J. Martins, J. Vieira, K. M. Schoeffler, R. A. Fonseca, and L. Silva, [arXiv:1812.06889](https://arxiv.org/abs/1812.06889); See also U. Sinha, J. Martins, J. Vieira, R. Fonseca, and L. Silva, in APS Meeting Abstracts, APS Division of Plasma Physics Meeting (2015), p. BO7.012. The approach of tracking particle trajectories from PIC simulation to compute the polarized radiation was first employed here, while the physical configuration and underlying physical processes are different in both cases.
- [17] A. Sagiv, E. Waxman, and A. Loeb, *Astrophys. J.* **615**, 366 (2004).
- [18] T. R. Boehly *et al.*, *Rev. Sci. Instrum.* **66**, 508 (1995).
- [19] M. Lobet, X. Davoine, E. d’Humières, and L. Gremillet, *Phys. Rev. Accel. Beams* **20**, 043401 (2017).
- [20] M. Lobet, C. Ruyer, A. Debayle, E. d’Humières, M. Grech, M. Lemoine, and L. Gremillet, *Phys. Rev. Lett.* **115**, 215003 (2015).
- [21] Extreme light infrastructure, <https://eli-laser.eu>.
- [22] Centre interdisciplinaire lumière extrême, <http://cilexsaclay.fr>.
- [23] C. Huntington *et al.*, *Nat. Phys.* **11**, 173 (2015).
- [24] G. Sarri *et al.*, *Nat. Commun.* **6**, 6747 (2015).
- [25] G. Sarri *et al.*, *Phys. Rev. Lett.* **110**, 255002 (2013).
- [26] G. Fiksel, W. Fox, A. Bhattacharjee, D. H. Barnak, P.-Y. Chang, K. Germaschewski, S. X. Hu, and P. M. Nilson, *Phys. Rev. Lett.* **113**, 105003 (2014).
- [27] W. Fox, G. Fiksel, A. Bhattacharjee, P. Y. Chang, K. Germaschewski, S. X. Hu, and P. M. Nilson, *Phys. Rev. Lett.* **111**, 225002 (2013).
- [28] J. Warwick *et al.*, *Phys. Rev. Lett.* **119**, 185002 (2017).
- [29] D. D. Ryutov, *Phys. Plasmas* **25**, 100501 (2018); D. D. Ryutov, N. L. Kugland, H. S. Park, C. Plechaty, B. A. Remington, and J. S. Ross, *Plasma Phys. Controlled Fusion* **54**, 105021 (2012).
- [30] J. Derouillat *et al.*, *Comput. Phys. Commun.* **222**, 351 (2018).
- [31] Higher number, *e.g.*, 100 particles per cell produced similar results.
- [32] M. Lyutikov, V. I. Pariev, and R. D. Blandford, *Astrophys. J.* **597**, 998 (2003).
- [33] C. T. Huynh and C.-M. Ryu, *Phys. Plasmas* **23**, 032127 (2016).
- [34] CASPER stands for Coherence and Spectral Postprocessor for Emitted Radiation. It can be directly used to postprocess radiation from PIC codes SMILEI and EPOCH.
- [35] L. Sironi and A. Spitkovsky, *Astrophys. J. Lett.* **707**, L92 (2009).
- [36] M. Chen, E. Esarey, C. G. R. Geddes, C. B. Schroeder, G. R. Plateau, S. S. Bulanov, S. Rykovanov, and W. P. Leemans, *Phys. Rev. ST Accel. Beams* **16**, 030701 (2013).
- [37] J. L. Martins, S. F. Martins, R. A. Fonseca, and L. O. Silva, *Proc. SPIE Int. Soc. Opt. Eng.* **7359**, 73590V (2009).
- [38] See Supplemental Material at <http://link.aps.org/supplemental/10.1103/PhysRevLett.122.204801> for the average kinetic energy of the selected particles were comparable to that of the entire respective beam species.
- [39] M. Born, E. Wolf, A. B. Bhatia, and P. Clemmow, *Principles of Optics: Electromagnetic Theory of Propagation, Interference and Diffraction of Light* (Pergamon Press, Oxford, 1970), Vol. 4.
- [40] It may be noted that these Stokes parameters are defined for a monochromatic wave and their applicability to an ensemble of plasma particles considered here is facilitated by the random phase approximation; see Ref. [12].
- [41] This importance of generation of circular polarization and its relevance to GRBs is discussed later.
- [42] A. Gruzinov and E. Waxman, *Astrophys. J.* **511**, 852 (1999).
- [43] Z. Li and E. Waxman, *Astrophys. J.* **651**, 328 (2006).
- [44] R. Svensson, *Astrophys. J.* **258**, 321 (1982).
- [45] We carried out PIC simulations by including the Landau-Lifshitz radiation reaction force and found results to be unchanged in agreement with Ref. [46]. Also plasma collisions are ignored due to lower plasma density employed in PIC simulations.
- [46] M. D’Angelo, L. Fedeli, A. Sgattoni, F. Pegoraro, and A. Macchi, *Mon. Not. R. Astron. Soc.* **451**, 3460 (2015).